coatings

MDPI

Article

Low Deposition Temperature-Induced Changes of the Microstructure and Tribological Property of WS_2 Film

Ming Hu [1], Yi Dong [2], Yan Wang [3], Desheng Wang [1,*], Dong Jiang [1], Yanlong Fu [1], Lijun Weng [1], Jiayi Sun [1] and Xiaoming Gao [1,*]

1 State Key Laboratory of Solid Lubrication, Lanzhou Institute of Chemical Physics, Chinese Academy of Sciences, Lanzhou 730000, China; hum413@lzb.ac.cn (M.H.); jiangd@licp.cas.cn (D.J.); fyanl@licp.cas.cn (Y.F.); wenglj@licp.cas.cn (L.W.); sunjy@licp.cas.cn (J.S.)
2 Shanghai Aerospace System Engineering Institute, Shanghai 201108, China; bert.dy@126.com
3 China Academy of Space Technology, Beijing 100094, China; yanzi2008hehe@126.com
* Correspondence: wangdsh@licp.cas.cn (D.W.); gaoxm@licp.cas.cn (X.G.); Tel.: +86-931-4968-071 (D.W.); +86-931-4968-091 (X.G.)

Received: 28 February 2019; Accepted: 27 March 2019; Published: 30 March 2019

Abstract: Pure WS_2 films were prepared by the radio frequency sputtering of a WS_2 target with the initial substrate temperature controlled to −40, −25, 0 °C and room temperature by cooling the holder with liquid nitrogen, respectively. The influence of the substrate temperature on the microstructures and the tribological properties of the prepared films have been evaluated and the wear mechanism of the films was explained. It revealed that with decreasing the substrate temperature, the prepared WS_2 film changed from the loose and coarse columnar plate structure for film deposited at room temperature to a much more compact morphology for film deposited at −40 °C. The WS_2 film deposited at low temperature of −40 or −25 °C exhibited a long wear life higher than 5.0×10^5 sliding cycles, while this was about 1.5×10^5 cycles for the WS_2 deposited at room temperature. The improved tribological properties for the low temperature-deposited film were mainly attributed to the much lower wear rate resulted from the compact structure as well as the sustained and steadily formed transform layer on the counterpart ball.

Keywords: tungsten disulfide; low temperature deposition; tribological property; wear life

1. Introduction

Sputtered transitional metal dichalcogenide (TMD) coatings, such as MoS_2 and WS_2, have been extensively investigated and applied as a super low friction lubricating materials for aerospace applications due to their excellent lubrication behavior especially under high vacuum conditions [1–5]. It has been investigated that the microstructure and the chemical composition of the deposited TMD films have a crucial effect on the friction coefficient and the wear life. Typically, the related characterization of the TMD films were controlled mainly by the deposition parameters, such as work pressure, substrate bias and substrate temperature [6–8]. However, the pure TMD films deposited at room temperature or a higher temperature exhibited a growth of the columnar plate structure. The coarse columnar plates constituted TMD films failed early during the friction and showed a very limited lifetime [9–11]. The poor wear resistance and short wear life of pure MoS_2 or WS_2 coatings limited their service in present and future long-life aerospace applications.

At present, modifying the microstructure by doping the TMD film with other elements or constructing multilayer structures is a conventional way to improve the tribological property of the TMD-based lubricating films It has been reported that the incorporation of metals or non-metallic elements and components into the TMD films helps in constricting a much denser structure and

reducing the wear rate of the films [12–18]. The multilayer architecture, controlled by alternating the nanometer-thick layer of MoS_2 or WS_2 and metal or compounds layer, has also been investigated to improve the tribological properties by the adjusting of the film microstructure and stress distribution [19–23]. Other novel designs of the pure TMD films for improving the tribological property were also investigated. It has been reported that the tribological property of the TMD film showed a significant improvement, especially exhibiting a long lubricating life, by depositing the pure TMD films onto the textured substrate or textured coatings [24–27]. The morphology of textured substrate or coating has a great influence on the growth of the pure TMD film and the optimized structure play an advantageous effect to achieve both the low friction coefficient and long wear life. The effect of the substrate temperature, another influence factor for the growth of the film, has long been investigated. However, previous research mainly focused on the effect of substrate temperature higher than room temperature on the microstructure and the friction coefficient of the TMD film [7,27–30]. The TMD film deposition at cryogenic temperature was rarely investigated. Spalvins [30] reported the sputtered MoS_2 film deposited at −195 °C have no lubricating characteristics due to the amorphous structure while MoS_2 film deposited at ambient or high temperature exhibited a well crystallized structure and low friction coefficient. Up to now, very little research has been done on the transitional region of the TMD film deposited at lower substrate temperature than ambient temperature.

In this paper, pure WS_2 films were deposited at substrate temperature range from −40 to 20 °C. The purpose of this article is to figure out the changes of the microstructure for the WS_2 deposited at different temperatures and to investigate the improvement of the tribological properties as well as the wear mechanism for the low temperature-deposited film.

2. Experiment

2.1. Sample Preparation

Pure WS_2 films were prepared by the radio frequency sputtering of one WS_2 target (76.2 mm in diameter, 99.9% in purity) at different low substrate temperatures controlled by a sample holder cooled by liquid nitrogen as illustrated elsewhere [31]. Commercially mechanically polished stainless steel (AISI 440C, $R_a \leq 0.02$ μm) and Si wafer were used as the substrates. Prior to deposition, the vacuum chamber was evacuated to a base pressure of 3.0×10^{-3} Pa, and then the substratesurfaces were Ar plasma bombarded for 20 min with a bias voltage of −600 V at a pressure of 2.0 Pa. Subsequently, the temperature of the substrate was controlled by cooling the substrate holder with a stable flow rate of liquid nitrogen. Through adjusting the flow rate of the liquid nitrogen, the substrate temperature was controlled to a stable temperature of −40, −25, 0 °C before the film deposition, respectively. When the substrate temperature was stabilized to the aimed value, the WS_2 film was deposited by the radio frequency sputtering of the WS_2 target with a power of 300 W under a working pressure of 2.0 Pa controlled by the flow rate of Ar with 30 min. The flow rate of the cooled liquid nitrogen remained unchanged during the film deposition while the substrate temperature was spontaneously increased due to the ion bombardment. The WS_2 film deposited at room temperature of about 20 °C was also deposited without the liquid nitrogen cooling while other conditions were not changed. The WS_2 films deposited at temperatures of −40, −25, 0 °C and room temperature were named with WS_2-40, WS_2-25, WS_2-0 and WS_2-RT, respectively.

2.2. Film Characterization and Tribological Measurements

The morphologies of WS_2 films deposited at different temperatures were characterized by high-resolution field emission scanning electron microscopy (FE-SEM, Hitachi SU8020, Tokyo, Japan) and a transmission electron microscope (TEM, JEOL 2100F, Tokyo, Japan). The crystal structures of the films were examined with an X-ray diffraction (XRD, X'Pert Pro, PANalytical Co., Almelo, The Netherland; 40 kV) with 1.54 Å Cu Kα radiation under an incident beam angle of 3°. The tribological properties of the prepared films were tested on a standard ball-on-disk tribometer

(WTM-2E, Lanzhou Institute of Chemical Physics, Lanzhou, China) under vacuum (<5.0 × 10^{-3} Pa) at room temperature. The counterpart was AISI 440C steel ball of 8 mm in diameter. The sliding speed was 1000 r/min with a rotational radius of 8 mm, corresponding to a linear speed of about 0.84 m s^{-1}, and the normal load was 5 N corresponding to a maximum Hertz contact stress of 1.0 GPa. After friction tests, the morphology of the wear track were analyzed by a MicroXAM3D non-contact surface profiler (AD Corporation, Cambridge, MA, USA). The wear rates (K) after the sliding tests were calculated via equation of $K = V/(FS)$, where V is the wear volume loss (mm^3), F is normal load (N), and S is total sliding distance (m). Raman signals for the wear track and the counterpart surface were also detected by a Horiba LabRAM HR Evolution spectrometer (Paris, France) with an excitation light source of wavelength 532 nm.

3. Results and Discussion

The high-resolution surface scanning electron microscope (SEM) images of the sputtered WS_2 films deposited under different substrate temperatures are shown in Figure 1. It can be seen that all the WS_2 films generally showed an acicular-like surface with curly columnar platelets. Typically, the sputtered WS_2 or MoS_2 films deposited at room temperature or high temperature exhibited a columnar plate Zone 2 morphology (Thornton model), which showed inherent porosity, as reported in other literatures [27,32]. It can be seen that the WS_2 film deposited at room temperature exhibited a loose coarse columnar structure as shown in Figure 1d, similarly to the films investigated by other researchers. While for the film deposited at lower temperatures, a much denser surface was occurred. The width of each columnar plate showed an increase with the increase of the substrate temperature. The mean widths for each of the columnar plate of the deposited WS_2 films were 180, 330, 380 and 650 nm for the films deposited at initial temperature of −40, −25, 0 and 20 °C, respectively. The featured porous structure of the sputtered WS_2 film could be greatly suppressed and a more compact structure would be achieved at the lower deposition temperature due to the change of the nucleation during film growth [30].

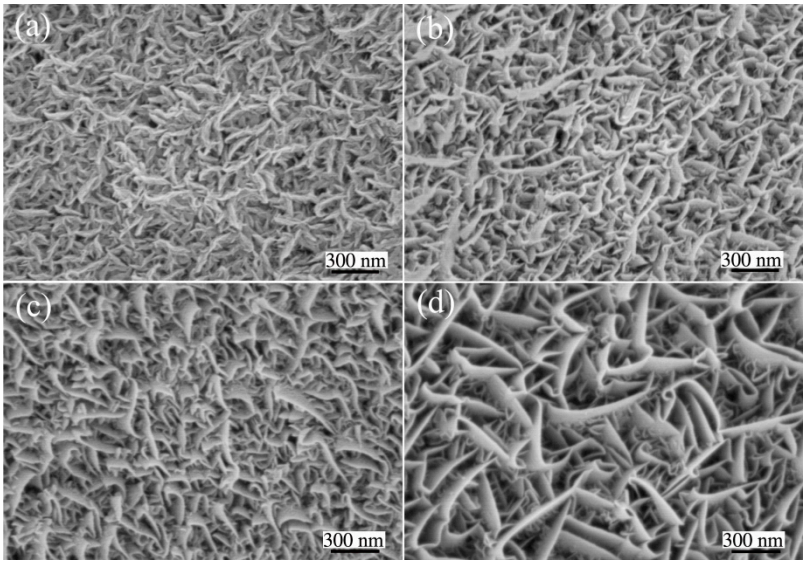

Figure 1. Surface scanning electron microscope (SEM) images of the WS_2 films deposited at different substrate temperature: (**a**) WS_2-40; (**b**) WS_2-25; (**c**) WS_2-0; and (**d**) WS_2-RT.

The integral and high-resolution cross-sectional SEM images of WS_2 film deposited at temperature of −40 °C are shown in Figure 2a,b, while that of WS_2 film deposited at room temperature is shown in Figure 2c,d. The thickness of the deposited film was controlled to be about 2.2 μm. It can be seen that the WS_2 film exhibited an obvious duplex layer microstructure composed of a very dense layer (approximately 200 nm) near the substrate and a columnar platelet one above for the

WS_2 film deposited either at low temperature or at room temperature. However, the upper columnar layers differed greatly under the influence of the substrate temperature. When the film deposited at initial substrate temperature of 20 °C, the columnar layers of the deposited WS_2 exhibited a cluster of almost independent coarse columnar plates with a large porosity among the plates. While for the film deposited at initial substrate temperature of −40 °C, the columnar layers showed a more compact structure with the columnar plates tightly connected with each other, and thus possess a minor porosity compared to the WS_2 film deposited at room temperature.

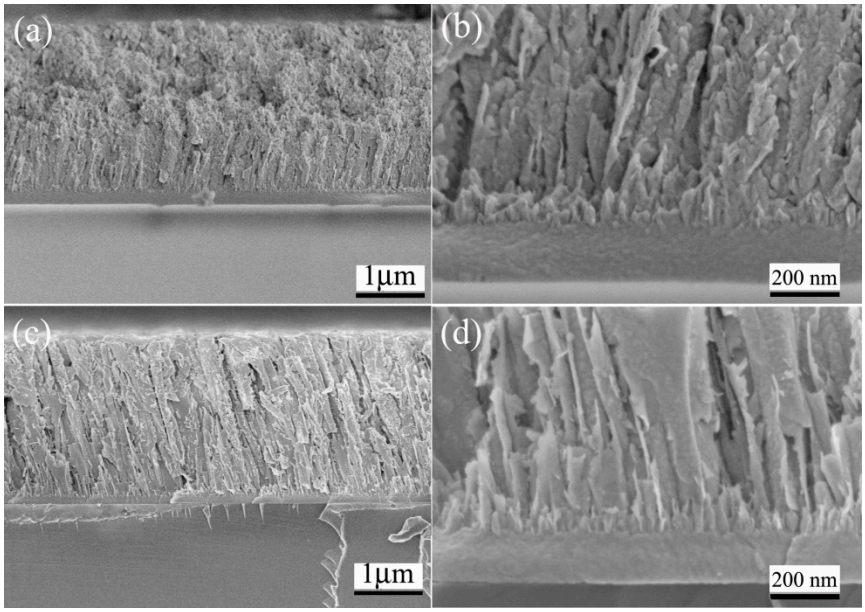

Figure 2. The cross-sectional SEM images under different magnifications for (**a**,**b**) WS_2-40 film and (**c**,**d**) WS_2-RT films.

Figure 3 shows the X-ray diffraction (XRD) spectra of the WS_2 films deposited at different substrate temperatures. The as-deposited WS_2 films exhibited hcp-WS_2 (002), (101), (103), and (112) diffraction peaks [27,33]. All the WS_2 films are crystalline with a predominantly (101) texture combined along with different intensity of (002), (103) and other diffraction peaks. Generally, the WS_2 film deposited at low temperature of −40 °C exhibited remarkable (002) peaks and a weak (103) peak. With the initial substrate temperature increased from −40 to 20 °C, the intensity of (002) peak gradually became weaker and weaker and nearly difficult to detect while the intensity of (103) peak increased drastically. Meanwhile, the intensity of the (101) peak was much higher for WS_2 film deposited at lower temperature. The XRD results indicated that the crystalline features of the WS_2 films were different with the substrate temperature during film deposition.

To further elucidate the effect of the substrate temperature on the microstructure of the deposited WS_2 films, the cross-sectional TEM images were performed and typical results for WS_2-40 and WS_2-RT films are shown in Figure 4. The overview TEM images of the Focused ion beam (FIB)-prepared slice showed that a much compact structure for the WS_2-40 film while a much loose structure for the WS_2-RT film, corresponding to the results derived from the SEM. For the WS_2 film deposited at room temperature, the initial growth of the WS_2 showed a crystalline structure with (002) basal domains with both c-axis orientated parallel and perpendicular to the substrate as shown in Figure 4a2. However, the top layer of the WS_2 exhibited a dominant (002) plane with *d*-spacing about 0.66 nm and the basal plane was perpendicular to the substrate surface, indicating a Type I structure [17,32]. For the WS_2 film deposited at low temperature of −40 °C, the region near the substrate showed a main amorphous phase with some crystalline WS_2 grains as can be seen from Figure 4b2. It was further determined from a selected area electron diffraction (SAED) pattern with rings that are somewhat diffuse. The top layer of the WS_2-40 film exhibited a well-crystallized structure as can be determined from both the

TEM image and the SAED pattern in Figure 4b2. It can be seen that the (002) crystalline plane was much more paralleled to the substrate for the WS_2-40 film compared to the WS_2-RT. Thus, the detected intensity of (002) peak from the XRD decreased while the intensity of the (103) peak increased with the increase of the deposition temperature for the WS_2 films due to the change of the direction of the (002) crystalline plane. The larger intensity of (101) for the WS_2-25 and WS_2-40 was mainly attributed to the much more compact structure.

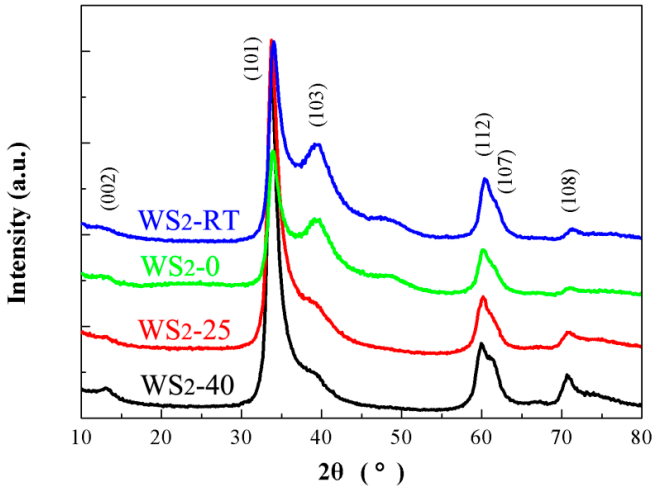

Figure 3. X-ray diffraction (XRD) patterns of the sputtered WS_2 films deposited at different substrate temperature: WS_2-40; WS_2-25; WS_2-0; and WS_2-RT.

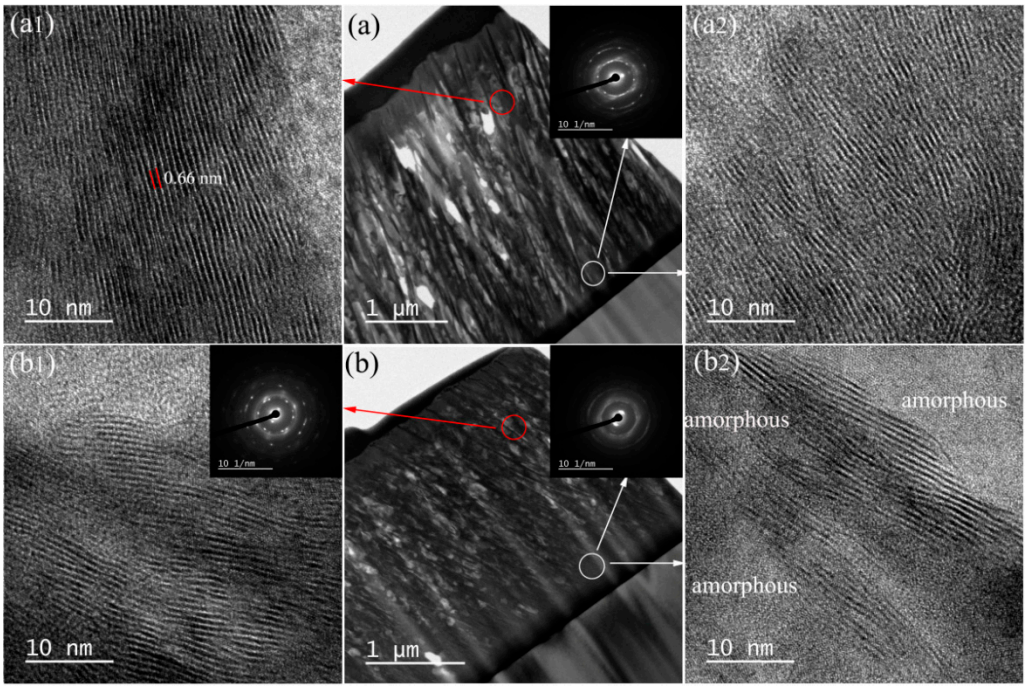

Figure 4. The cross-sectional high-resolution transmission electron microscope (HRTEM) images of WS_2 film: (**a**,**a1**,**a2**) an overview of FIB-prepared slice of the WS_2-RT and the magnified image of the selected regions; (**b**,**b1**,**b2**) an overview of FIB-prepared slice of the WS_2-40 and the magnified image of the selected regions. The insets are the selected area electron diffraction (SAED) pattern of the marked area.

The typical friction coefficients of the WS_2 films deposited at different substrate temperatures are shown in Figure 5. The tribotest was stopped when the friction coefficient of the film reached to 0.2 due to the film failure. In general, it showed that the wear life of the WS_2 film exhibited a significant increase with the decrease of the initial substrate temperature. The WS_2 film deposited at room temperature showed a limited wear life less than 1.5×10^5 sliding cycles. With the substrate temperature decrease to 0 °C, the changes of the fiction coefficients was similar to that of WS_2-RT, exhibiting a low and minor fluctuating friction coefficient in the initial cycles and then an increased and much fluctuating friction coefficient until the film failure. The wear life of the WS_2-0 film was limited to about 2.5×10^5 sliding cycles. When the substrate temperature was set to a lower value of −40 and −25 °C, the prepared WS_2 films exhibited much improved tribological performances. The friction coefficients showed a minor fluctuate with a low mean value below 0.03 in the initial 1.0×10^5 sliding cycles. Afterward, the friction coefficient showed a much minor fluctuation and gradually increased to a higher value about 0.07. For both WS_2-25 and WS_2-40 films, the wear lives were higher than 5.0×10^5 sliding cycles.

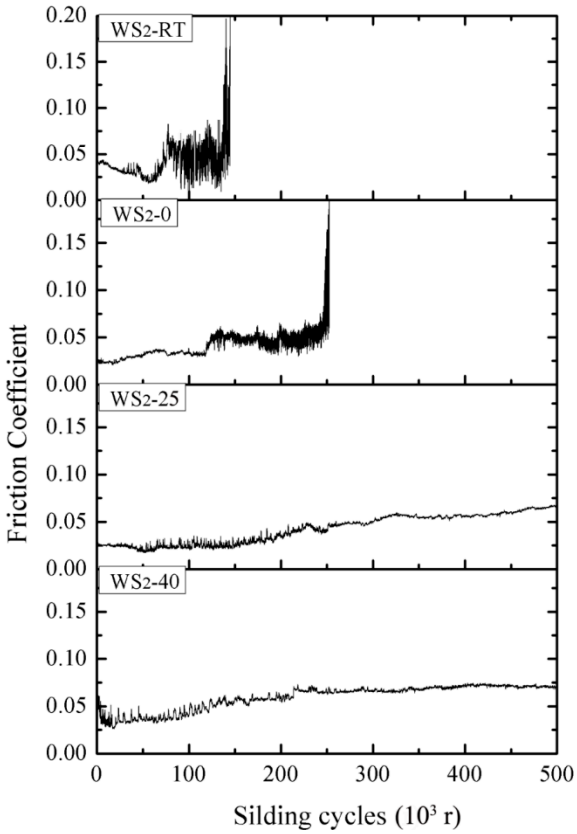

Figure 5. Typical friction curves of the WS_2 films deposited at different substrate temperatures.

In order to deeply understand the wear mechanism of the WS_2 films deposited at different temperatures, the 3D profile images of the wear track for the WS_2 films after 1.0×10^5 sliding cycles were detected and shown in Figure 6. It can be seen that a most narrow and shallow wear track was appeared for the WS_2-40 films. While with the increase with the substrate temperature, the wear track of prepared WS_2 film exhibited a much more depth with the increase of the substrate temperature. The calculated wear rates were 0.23×10^{-6}, 0.40×10^{-6}, 0.44×10^{-6} and 1.35×10^{-6} $mm^3\ N^{-1}\ m^{-1}$ for the WS_2-40, WS_2-25, WS_2-0 and WS_2-RT, respectively. Obviously, the wear rate for the WS_2 films increased when raising the substrate temperature.

The Raman spectra at the center of the wear track and the transform layer on the counterpart after 1.0×10^5 sliding cycles and the end of the tribotest were detected as shown in Figure 7. It can be seen that Raman modes with peaks centered at 347, 420 and 524 cm^{-1} for E_{2g}, A_{1g} and second order Raman modes of WS_2 [33,34], respectively, were detected after 1.0×10^5 liding cycles from the wear track for both WS_2-40 and WS_2-RT films, indicating that the films were not worn out. However, the intensity of the Raman signal of the transform layer on the counterpart for the WS_2-RT was much lower than that of WS_2-40. Afterward, the friction coefficient of the WS_2-RT increased to above 0.05 and fluctuated drastically until film lubricating failure for 1.0×10^5 sliding cycles as shown in Figure 5. In contrast, well-formed transform layer on the counterpart ball after 1.0×10^5 or 5.0×10^5 sliding cycles was detected by the Raman spectra for the WS_2-40 as can be seen in Figure 7b, indicating a superior lubricating state corresponding to the stable friction curves shown in Figure 5.

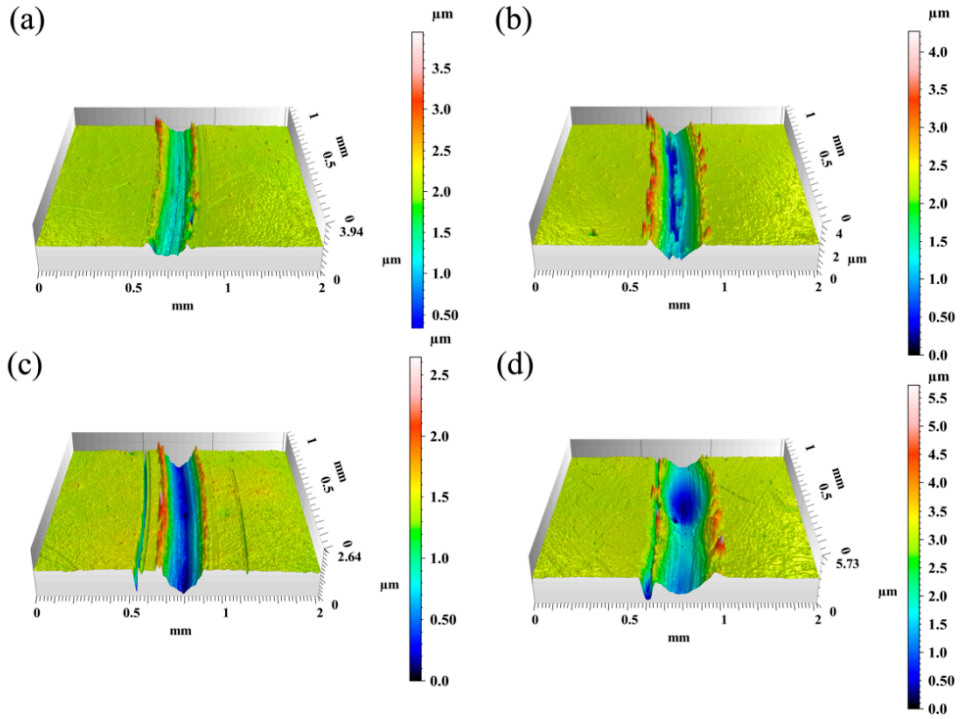

Figure 6. Typical 3D profile images of the wear tracks after sliding 1.0×10^5 cycles in vacuum for (**a**) WS_2-40, (**b**) WS_2-25, (**c**) WS_2-0, and (**d**) WS_2-RT.

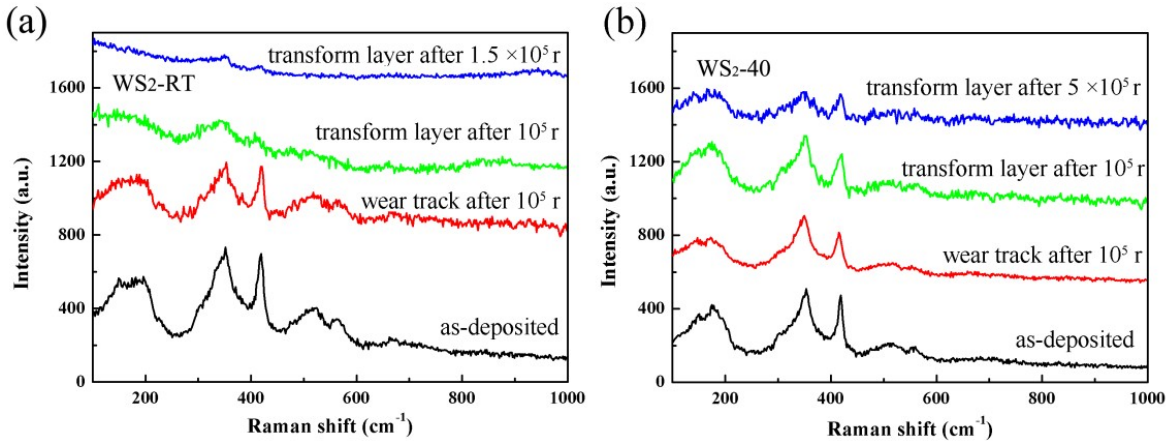

Figure 7. Raman spectra of the as-deposited film, wear track and transform layer on counterpart ball after1.0×10^5 sliding cycles as well as after film failure or 5.0×10^5 sliding cycles for (**a**) WS_2-RT and (**b**) WS_2-40 films.

Finally, pure WS_2 films with different microstructures have been prepared by the sputtering technology through adjusting the initial substrate temperature cooled by the liquid nitrogen. With the substrate temperature decreasing from room temperature to −40 °C, the morphology of the deposited film gradually changed from loose and coarse columnar structure to a much more compact tiny columnar structure, which generally corresponded to the columnar plate Zone 2 morphology. Although the substrate temperature increased due to the ion bombardment during film deposition, the film deposited at lower initial substrate temperature continued the original compact structure. However, changes of the crystallinity along the film thickness were different for the low temperature-deposited film. The WS_2-40 film changed from a predominant amorphous structure at the bottom layer to a mainly well crystallized structure at the top layer while the WS_2 film deposited at room temperature exhibited a high crystallinity through the whole film as can be seen from Figure 4.

For the pure WS_2 thin film with loose columnar plate morphology deposited at room temperature, the occurrence of the deformation/fracture of the columnar plates would happen and only partly rearrangement of the fragmentized plates contributed as an effective lubricating layer to provide low friction coefficient during the sliding friction [24,35]. Thus the WS_2-RT exhibited a higher wear rate and a limited wear life. While for the WS_2 film deposited at lower initial substrate temperature of −40 °C, the much more compact structure could largely suppress the fracture of the tiny columnar of WS_2 and resulted in a much lower wear rate nearly one sixth of that for WS_2-RT. The transform lubricating WS_2 layer on the counterpart ball plays a great role on the tribological property of the WS_2 film [36,37]. Compared to the WS_2 film deposited at room temperature, the well-ordered transform lubricating WS_2 layer would form on the counterpart ball for the WS_2 film deposited at lower initial substrate temperature of −40 °C, as shown in Figure 7. For the WS_2 film deposited at room temperature, the (002) crystalline plane totally perpendicular to the substrate as well as the drastic fracture of the columnar plates would be adverse for the formation of the transform lubricating layer. While for the WS_2 film deposited at low temperature, both the compact structure and much more paralleled (002) crystalline plane to the substrate, compared to the WS_2-RT, was beneficial for the transforming of the lubricating layer onto the counterpart ball and further maintaining a better lubricating state and a less-fluctuant friction coefficient. Due to the low crystalliinity of the bottom layer, the friction coefficient of the WS_2-40 film showed a gradual increase to about 0.07 after 5.0×10^5 sliding cycles, still maintaining a good lubricating state, which is mainly attributed to the well-formed sustained transform layer as detected by the Raman spectrum.

4. Conclusions

In summary, pure WS_2 films were prepared by radio frequency sputtering technology by controlling the initial substrate temperature from room temperature to −40 °C. This showed that the initial substrate temperatures have a great influence on the microstructure and tribological property of the prepared films. With decreasing the substrate temperature from room temperature to −40 °C, the prepared WS_2 film changed from the loose and coarse columnar plate structure to a much more compact morphology. The wear rates of the deposited WS_2 films showed a great reduction with decreasing substrate temperature. WS_2 film deposited at −40 °C exhibited a lowest wear rate of 0.23×10^{-6} mm^3 N^{-1} m^{-1}, nearly one sixth of that for WS_2 film obtained at room temperature. The WS_2 film deposited at low temperature of −40 or −20 °C exhibited a long wear life higher than 5.0×10^5 sliding cycles while this was only 1.5×10^5 sliding cycles for the WS_2 deposited at room temperature. Both the compact structure resulted in a lower wear rate and the sustained formed transform layer on the counterpart ball contributed to the improved tribological properties for the low temperature-deposited WS_2 films.

Author Contributions: Conceptualization, D.W. and X.G.; Formal Analysis, Y.D., Y.W., and Y.F.; Methodology, M.H., Y.D., D.W., and D.J.; Supervision, L.W., and J.S.; Validation, J.S. and X.G.; Writing—Original Draft, M.H. and D.W.; Writing—Review and Editing, D.W. and X.G.

Funding: This research was financially supported by the National Natural Science Foundation of China (Nos. 51575508, 51575509 and 51875551).

Conflicts of Interest: The authors declare no conflict of interest.

References

1. Banerjee, T.; Chattopadhyay, A. Influence of substrate bias on structural and tribo-mechanical properties of pulsed magnetron sputtered TiN–WS_x hard-lubricious coating. *Tribol. Int.* **2018**, *123*, 81–91. [CrossRef]
2. Luo, T.; Wang, P.; Qiu, Z.; Yang, S.; Zeng, H.; Cao, B. Smooth and solid WS_2 submicrospheres grown by a new laser fragmentation and reshaping process with enhanced tribological properties. *Chem. Commun.* **2016**, *52*, 10147–10150. [CrossRef] [PubMed]
3. Scharf, T.; Prasad, S.; Dugger, M.; Kotula, P.; Goeke, R.; Grubbs, R. Growth, structure, and tribological behavior of atomic layer-deposited tungsten disulphide solid lubricant coatings with applications to MEMS. *Acta Mater.* **2006**, *54*, 4731–4743. [CrossRef]
4. Zeng, Y.; He, F.; Wang, Q.; Yan, X.; Xie, G. Friction and wear behaviors of molybdenum disulfide nanosheets under normal electric field. *Appl. Surf. Sci.* **2018**, *455*, 527–532. [CrossRef]
5. Scharf, T.W.; Prasad, S.V. Solid lubricants: A review. *J. Mater. Sci.* **2013**, *48*, 511–531. [CrossRef]
6. Bulbul, F.; Efeoğlu, I.; Arslan, E.; Efeoglu, I. The effect of bias voltage and working pressure on S/Mo ratio at MoS_2–Ti composite films. *Appl. Surf. Sci.* **2007**, *253*, 4415–4419. [CrossRef]
7. Shi, J.P.; Tong, R.; Zhou, X.B.; Gong, Y.; Zhang, Z.P.; Ji, Q.Q.; Zhang, Y.; Fang, Q.Y.; Gu, L.; Wang, X.N.; et al. Temperature-mediated selective growth of MoS_2/WS_2 and WS_2/MoS_2 vertical stacks on Au foils for direct photocatalytic applications. *Adv. Mater.* **2016**, *28*, 10664. [CrossRef]
8. Arslan, E.; Totik, Y.; Efeoglu, I. Comparison of structure and tribological properties of MoS_2–Ti films deposited by biased-dc and pulsed-dc. *Prog. Org. Coat.* **2012**, *74*, 772–776. [CrossRef]
9. Gustavsson, F.; Jacobson, S.; Cavaleiro, A.; Polcar, T. Ultra-low friction W–S–N solid lubricant coating. *Surf. Coat. Technol.* **2013**, *232*, 541–548. [CrossRef]
10. Polcar, T.; Gustavsson, F.; Thersleff, T.; Jacobson, S.; Cavaleiro, A. Complex frictional analysis of self-lubricant W–S–C/Cr coating. *Faraday Discuss.* **2012**, *156*, 383–401. [CrossRef] [PubMed]
11. Xu, S.; Sun, J.; Weng, L.; Hua, Y.; Liu, W.; Neville, A.; Hu, M.; Gao, X. In-situ friction and wear responses of WS2 films to space environment: Vacuum and atomic oxygen. *Appl. Surf. Sci.* **2018**, *447*, 368–373. [CrossRef]
12. Singh, H.; Mutyala, K.C.; Mohseni, H.; Scharf, T.W.; Evans, R.D.; Doll, G.L. Tribological performance and coating characteristics of sputter deposited Ti doped MoS_2 in rolling and sliding contact. *Tribol. Trans.* **2015**, *58*, 767–777. [CrossRef]
13. Hsu, K.W.; Zhu, Y.; Yao, N.; Firth, S.; Clark, R.; Kroto, H.W.; Walton, D. Titanium-doped molybdenum disulfide nanostructures. *Adv. Funct. Mater.* **2001**, *11*, 69–74. [CrossRef]
14. Strapasson, G.; Badin, P.C.; Soares, G.V.; Machado, G.; Figueroa, C.A.; Hubler, R.; Gasparin, A.L.; Baumvol, I.J.R.; Aguzzoli, C.; Tentardini, E.K. Structure, composition, and mechanical characterization of dc sputtered TiN–MoS_2 nanocomposite thin films. *Surf. Coat. Technol.* **2011**, *205*, 3810–3815. [CrossRef]
15. Scharf, T.; Kotula, P.; Prasad, S.; Kotula, P. Friction and wear mechanisms in MoS_2/Sb_2O_3/Au nanocomposite coatings. *Acta Mater.* **2010**, *58*, 4100–4109. [CrossRef]
16. Stoyanov, P.; Chromik, R.R.; Goldbaum, D.; Lince, J.R.; Zhang, X. Microtribological performance of Au–MoS_2 and Ti–MoS_2 coatings with varying contact pressure. *Tribol. Lett.* **2010**, *40*, 199–211. [CrossRef]
17. Arslan, E.; Bulbul, F.; Alsaran, A.; Çelik, A.; Efeoglu, I. The effect of deposition parameters and Ti content on structural and wear properties of MoS_2Ti coatings. *Wear* **2005**, *259*, 814–819. [CrossRef]
18. Lince, J.R. Tribology of Co-sputtered Nanocomposite Au/MoS_2 solid lubricant films over a wide contact stress range. *Tribol. Lett.* **2004**, *17*, 419–428. [CrossRef]
19. Shang, K.; Zheng, S.; Ren, S.; Pu, J.; He, D.; Liu, S. Improving the tribological and corrosive properties of MoS_2-based coatings by dual-doping and multilayer construction. *Appl. Surf. Sci.* **2018**, *437*, 233–244. [CrossRef]

20. Hu, J.; Bultman, J.; Zabinski, J. Microstructure and lubrication mechanism of multilayered MoS_2/Sb_2O_3 thin films. *Tribol. Lett.* **2006**, *21*, 169–174. [CrossRef]
21. Pimentel, J.V.; Polcar, T.; Cavaleiro, A. Structural, mechanical and tribological properties of Mo–S–C solid lubricant coating. *Surf. Coat. Technol.* **2011**, *205*, 3274–3279. [CrossRef]
22. Polcar, T.; Cavaleiro, A. Review on self-lubricant transition metal dichalcogenide nanocomposite coatings alloyed with carbon. *Surf. Coat. Technol.* **2011**, *206*, 686–695. [CrossRef]
23. Li, S.; Deng, J.; Yan, G.; Zhang, K.; Zhang, G. Microstructure, mechanical properties and tribological performance of TiSiN–WS_2 hard-lubricant coatings. *Appl. Surf. Sci.* **2014**, *309*, 209–217. [CrossRef]
24. Wang, D.; Hu, M.; Jiang, D.; Gao, X.; Fu, Y.; Sun, J.; Weng, L. Cabbage-like WS_2/Ni bilayer thin film for improved tribological property. *Surf. Coat. Technol.* **2019**, *358*, 50–56. [CrossRef]
25. Wang, D.; Hu, M.; Gao, X.; Jiang, D.; Fu, Y.; Weng, L.; Sun, J. Tailoring of the interface morphology of WS_2/CrN bilayered thin film for enhanced tribological property. *Vacuum* **2018**, *156*, 157–164. [CrossRef]
26. Arenas, M.A.; Ahuir-Torres, J.I.; García, I.; Carvajal, H.; de Damborenea, J. Tribological behaviour of laser textured Ti6Al4V alloy coated with MoS_2 and graphene. *Tribol. Int.* **2018**, *128*, 240–247. [CrossRef]
27. Scharf, T.; Rajendran, A.; Banerjee, R.; Sequeda, F. Growth, structure and friction behavior of titanium doped tungsten disulphide (Ti–WS_2) nanocomposite thin films. *Thin Solid Films* **2009**, *517*, 5666–5675. [CrossRef]
28. Bozheyev, F.; Valiev, D.; Nemkayeva, R. Pulsed cathodoluminescence and Raman spectra of MoS_2 and WS_2 nanocrystals and their combination MoS_2/WS_2 produced by self-propagating high-temperature synthesis. *Appl. Phys. Lett.* **2016**, *108*, 093111. [CrossRef]
29. Chen, F.; Wang, L.; Ji, X.; Zhang, Q. Temperature-dependent two-dimensional transition metal dichalcogenide heterostructures: controlled synthesis and their properties. *ACS Appl. Mater. Interfaces* **2017**, *9*, 30821–30831. [CrossRef] [PubMed]
30. Spalvins, T. Tribological properties of sputtered MoS_2 films in relation to film morphology. *Thin Solid Films* **1980**, *73*, 291–297. [CrossRef]
31. Gao, X.; Sun, J.; Fu, Y.; Jiang, D.; Wang, D.; Weng, L.; Hu, M. Improved wear resistance of WS_2 film by LT-deposited Ti interlayer with ω phase structure. *Vacuum* **2018**, *155*, 423–427. [CrossRef]
32. Hilton, M.R.; Jayaram, G.; Marks, L.D. Microstructure of cosputter-deposited metal- and oxide-MoS_2 solid lubricant thin films. *Tribol. Int.* **2011**, *13*, 1022–1032. [CrossRef]
33. Deepthi, B.; Barshilia, H.C.; Rajam, K.; Konchady, M.S.; Pai, D.M.; Sankar, J. Structural, mechanical and tribological investigations of sputter deposited CrN–WS_2 nanocomposite solid lubricant coatings. *Tribol. Int.* **2011**, *44*, 1844–1851. [CrossRef]
34. Perea-López, N.; Elías, A.L.; Berkdemir, A.; Castro-Beltran, A.; Gutiérrez, H.R.; Feng, S.; Lv, R.; Hayashi, T.; López-Urías, F.; Ghosh, S.; et al. Photosensor device based on few-layered WS_2 films. *Adv. Funct. Mater.* **2013**, *23*, 5511–5517. [CrossRef]
35. Moser, J.; Levy, F. MoS_{2-x} lubricating films: Structure and wear mechanisms investigated by cross-sectional transmission electron microscopy. *Thin Solid Films* **1993**, *228*, 257–260. [CrossRef]
36. Spalvins, T. Frictional and morphological properties of Au–MoS_2 films sputtered from a compact target. *Thin Solid Films* **1984**, *118*, 375–384. [CrossRef]
37. Zhang, X.; Qiao, L.; Chai, L.; Xu, J.; Shi, L.; Wang, P. Structural, mechanical and tribological properties of Mo–S–N solid lubricant films. *Surf. Coat. Technol.* **2016**, *296*, 185–191. [CrossRef]